Vol 453|29 May 2008|doi:10.1038/nature06964

LETTERS

Anatase TiO_2 single crystals with a large percentage of reactive facets

Hua Gui Yang[1]*, Cheng Hua Sun[1,2]*, Shi Zhang Qiao[1], Jin Zou[3], Gang Liu[1,4], Sean Campbell Smith[1,2], Hui Ming Cheng[4] & Gao Qing Lu[1]

Owing to their scientific and technological importance, inorganic single crystals with highly reactive surfaces have long been studied[1–13]. Unfortunately, surfaces with high reactivity usually diminish rapidly during the crystal growth process as a result of the minimization of surface energy. A typical example is titanium dioxide (TiO_2), which has promising energy and environmental applications[14–17]. Most available anatase TiO_2 crystals are dominated by the thermodynamically stable {101} facets (more than 94 per cent, according to the Wulff construction[10]), rather than the much more reactive {001} facets[8–13,18–20]. Here we demonstrate that for fluorine-terminated surfaces this relative stability is reversed: {001} is energetically preferable to {101}. We explored this effect systematically for a range of non-metallic adsorbate atoms by first-principle quantum chemical calculations. On the basis of theoretical predictions, we have synthesized uniform anatase TiO_2 single crystals with a high percentage (47 per cent) of {001} facets using hydrofluoric acid as a morphology controlling agent. Moreover, the fluorated surface of anatase single crystals can easily be cleaned using heat treatment to render a fluorine-free surface without altering the crystal structure and morphology.

The surface stability and reactivity of inorganic single crystals have long been thought to be dominated by their surface chemistry, whose effect on the equilibrium morphology is critical for the synthesis of single crystals with high reactivity[1–13,21]. For anatase TiO_2, both theoretical and experimental studies found that the minority {001} facets in the equilibrium state are especially reactive[8]. However, large high-quality anatase single crystals with a high percentage of {001} facets have not been synthesized[22–24]. An early study[23] showed that the hydrothermal treatment of hydrous titanium(IV) oxide in the presence of hydrofluoric acid resulted in irregular aggregates of polymorphic TiO_2 with anhedral morphology. Recently, anatase single crystals were synthesized using chemical transport reactions, but the process had a long reaction time and the crystals were of low purity and had no {001} facets[24]. Therefore, preparation of uniform, high-purity anatase single crystals with controllable crystallographic facets still remains a challenge.

To this end, attempts have been made with various adsorbate atoms to change the relative stabilities of different crystal facets[19–23]. For anatase TiO_2, among oxygenated surfaces, {100} facets are the most stable, whereas under clean and hydrogenated conditions, {101} facets are the most stable[5,10,21]. However, both H- and O-terminated anatase surfaces present high surface energies (γ), which restrict the formation of large anatase single crystals. High values of γ are mainly attributed to the high bonding energies (D_0) of H–H (436.0 kJ mol^{-1}) and O–O (498.4 kJ mol^{-1})[25]. Therefore, using a low-D_0 element with strong bonding to Ti might provide an

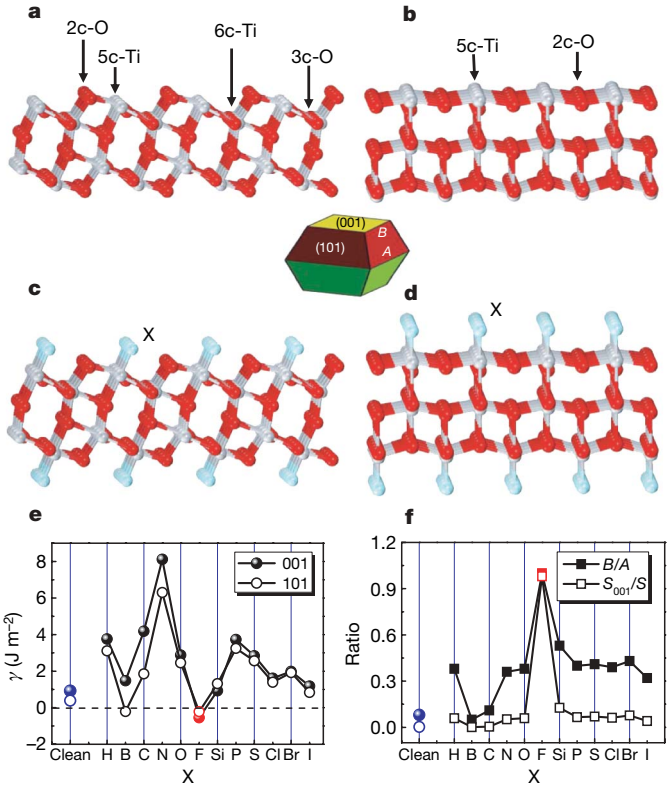

Figure 1 | Slab models and calculated surface energies of anatase TiO_2 (001) and (101) surfaces. The optimised ratios of B/A and percentage of {001} facets (S_{001}/S), where S and S_{001} are respectively the total surface area and that contributed by the {001} facets, are also shown. **a**, **b**, Unrelaxed, clean (001) and (101) surfaces. Ti and O atoms are represented by grey and red spheres, with sixfold Ti, fivefold Ti, threefold O and twofold O labelled as 6c-Ti, 5c-Ti, 3c-O and 2c-O, respectively. **c**, **d**, Unrelaxed (001) and (101) surfaces surrounded by adsorbate X atoms. **e**, Calculated energies of the (001) and (101) surfaces surrounded by X atoms. **f**, Plots of the optimized value of B/A and percentage of {001} facets for anatase single crystals with various adsorbate atoms X. In **e** and **f**, clean-surface results (denoted by blue spheres and circles) are used for reference. As indicated in the inset diagram, two independent parameters A and B denote lengths of the side of the bipyramid and the side of the square {001} 'truncation' facets, respectively. The ratio of highly reactive {001} facets to total surface area may therefore be described by the value of S_{001}/S or B/A (where $0 \leq B/A \leq 1$).

[1]ARC Centre of Excellence for Functional Nanomaterials, School of Engineering and Australian Institute for Bioengineering and Nanotechnology, [2]Centre for Computational Molecular Science, Australian Institute for Bioengineering and Nanotechnology, [3]Centre for Microscopy and Microanalysis and School of Engineering, The University of Queensland, Queensland 4072, Australia. [4]Shenyang National Laboratory for Materials Science, Institute of Metal Research, Chinese Academy of Sciences, 72 Wenhua Road, Shenyang 110016, China.
*These authors contributed equally to this work.

effective means for stabilizing the surfaces. Interestingly, F is such an element, as $D_0^{F-F} = 158.8\,kJ\,mol^{-1}$ (ref. 25) and $D_0^{F-Ti} = 569.0\,kJ\,mol^{-1}$ (ref. 26).

To further explore the effects of various adsorbate atoms, we carried out a systematic investigation of 12 non-metallic atoms X (where X can represent H, B, C, N, O, F, Si, P, S, Cl, Br or I) based on first-principle calculations. Figure 1a–d illustrates the models of clean and X-terminated (001) and (101) surfaces. The calculated γ values for different adsorbates are shown in Fig. 1e, from which two conclusions can be drawn: among the 12 X-terminated surfaces and the clean surfaces, termination with F atoms not only yields the lowest value of γ for both the (001) and (101) surfaces, but also results in (001) surfaces that are more stable than (101) surfaces.

These results indicate that it might be possible to achieve anatase TiO_2 single crystals with a high percentage of anatase {001} facets if their surfaces are surrounded by F atoms. Furthermore, on the basis of the shape-dependent thermodynamic model proposed in ref. 27, the optimized value of B/A (the length parameters illustrated in Fig. 1) and the percentage of {001} facets can be predicted if γ is known. Fig. 1f shows that the F-terminated surfaces have the highest degree of truncation ($B/A \rightarrow 1$ approximately); the F-terminated surfaces of anatase TiO_2 should therefore be dominated by {001} facets.

To verify these theoretical predictions, titanium tetrafluoride (TiF_4) aqueous solution and hydrofluoric acid were used as the anatase single crystals' precursor and crystallographic controlling agent, respectively, to generate the truncated anatase bipyramids. Representative scanning electron microscopy (SEM) images of the products synthesized with different concentrations of TiF_4 and reaction times are shown in Fig. 2a, d. On the basis of the symmetries of anatase TiO_2, the two flat, square surfaces must be {001} facets and the eight isosceles trapezoidal surfaces are {101} facets of the anatase TiO_2 single crystals (further evidence for this is in Fig. 3 and Supplementary Fig. 7). The yield of anatase TiO_2 single crystals is around 90%, even though some agglomerates and/or irregular particles (Supplementary Fig. 4) were occasionally observed.

To examine the uniformity of the synthesized anatase crystals, we statistically analysed the values of A and B/A under the different synthesis conditions. The results are presented in Fig. 2b, c, e, f: for the respective cases shown in Fig. 2a, d, the average values of A are 1.66 μm and 1.64 μm with relative standard deviations of 8.4% and 15.8% (Fig. 2b, e), and the degrees of truncation (given by B/A) are 0.77 and 0.84 with relative standard deviations of 4.3% and 5.1% (Fig. 2, f). We estimate the percentages of {001} facets to be 35% and 47%, respectively.

The fact that anatase single crystals generated with a low concentration of TiF_4 exhibit a high degree of truncation may be attributed to the higher fluorine density on the surface, which makes the isotropic growth more obvious. This is remarkably consistent with our theoretical predictions, and can be understood from the viewpoint of shape-control chemistry[20,21]. The free energy of (001) surfaces can be reduced to $0.51\,J\,m^{-2}$ using the (1×4) reconstruction[13], which suggests that this reconstruction could also stabilize (001) surfaces. However, on the basis of the values of γ calculated in ref. 13, the optimized value of B/A is around 0.37. This is very different from the values, 0.77 and 0.84, that we obtained in our experiments, indicating that the high percentage of {001} facets does not result from the (1×4) reconstruction. According to our detailed calculations based on a perfect (1×1) unit cell and (4×4) supercells of (001) surfaces (Supplementary Information Part I), all surfaces terminated with F atoms have very low values of γ. We therefore believe that the stabilization effect of F atoms is the essential reason for the percentage of {001} facets being as high as 47% in our experiments.

Regarding the stabilization mechanism, a detailed analysis of the surface geometries has been carried out (Supplementary Information Part I). Under clean conditions, the balance between the O–O repulsions and the attractive Ti–O π interactions is broken owing to the cleavage of surfaces, causing unsaturated O and Ti atoms to move outward (Supplementary Table 1). However, with the formation of Ti–F bonds, surface O and Ti atoms move inward and outward significantly, owing to the strong repulsive and attractive interactions

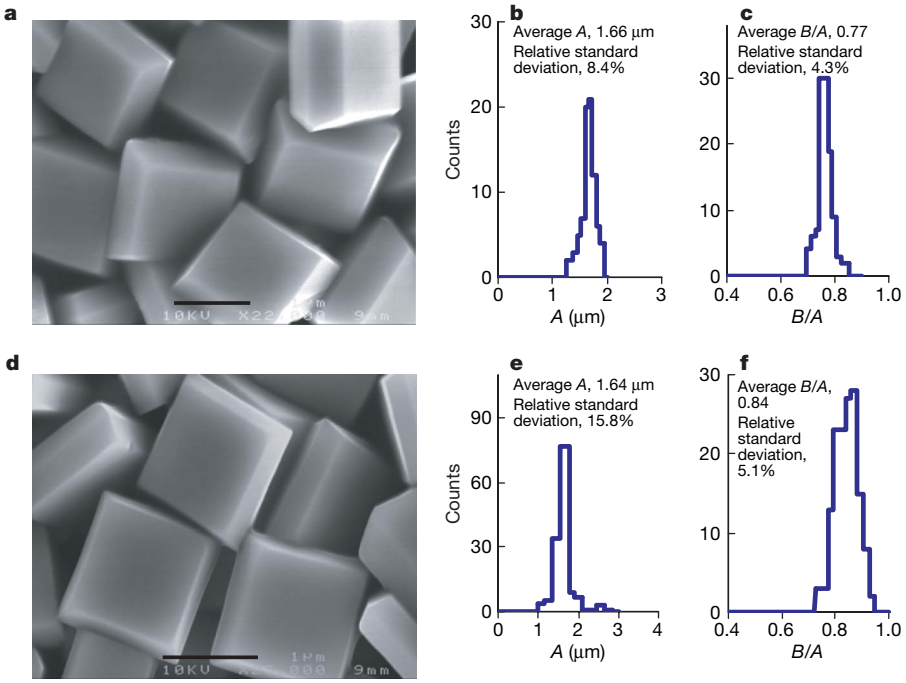

Figure 2 | SEM images and statistical data for the size and truncation degree of anatase single crystals. a, The morphology of anatase single crystals synthesized with 5.33 mM TiF_4 aqueous solution at 180 °C for 14 h. **b**, The size (A) distribution of anatase single crystals in **a**. **c**, The degree of truncation (B/A) of anatase single crystals in **a**. **d**–**f**, As in **a**–**c**, but for different synthesis conditions; the degree of truncation of anatase single crystals was controlled by halving the concentration of TiF_4 and extending the reaction time to 20 h. For both the size and the degree of truncation, the relative standard deviations of all statistical data were derived from counting more than 100 single crystals for each sample. Scale bars in **a** and **d**, 1 μm.

of O–F and Ti–F bonds, respectively. This analysis is consistent with the calculated electronic structures (see Supplementary Fig. 3) because the Ti_{3d} and O_{2p} electrons can both interact strongly with the F_{2p} electron. A new balance can thereby be established between O–O/F–O repulsions and Ti–O/Ti–F attractions, which stabilizes Ti and O atoms on the surfaces.

As a further confirmation, no crystal facet control was observed in the absence of hydrofluoric acid, and only hollow spherical polycrystalline anatase particles were formed (see Supplementary Fig. 5)[28]. Hydrofluoric acid is believed to have dual roles here: to retard hydrolysis of the titanium precursor and to reduce surface energy to promote the isotropic growth along the [010] and [100] axes[18,20], as illustrated in Fig. 1a–f. In comparison with the sample in Fig. 2a, the anatase single crystals obtained in shorter reaction times are of a smaller size and a higher degree of truncation (for example $A = 850$ nm and $B/A = 0.84$ at 8 h, depicted in Supplementary Fig. 6). According to the theoretical predictions (Fig. 1f), the B/A can be as great as 1.0 for the fully F-terminated surfaces; this important prediction indicates that ultrathin TiO_2 nanosheets may be synthesized.

Bright field images of transmission electron microscopy (TEM) and selected-area electron diffraction patterns confirm that each free-standing crystal shows single-crystal characteristics (Fig. 3a, b). The selected-area electron diffraction patterns can be indexed into diffraction spots of the [001] zone[28]. The high-resolution TEM image (Fig. 3c) shows the (200) and (020) atomic planes with a lattice spacing of 1.89 Å and an interfacial angle of 90° (ref. 28). A corresponding fast-Fourier-transform-filtered TEM image of tetragonal atomic arrangement on the (001) surface is shown in Fig. 3d. The interfacial angle between two parallel faces and other surrounding faces is 68.3° ± 0.3° on average (Supplementary Fig. 7); this value is identical to the theoretical value for the angle between the {001} and {101} facets of anatase[5].

In the X-ray diffraction pattern shown in Fig. 4a, all the diffraction peaks match well with the crystal structure of the anatase TiO_2 phase (space group $I4_1/amd$)[28]. The X-ray photoelectron spectrum of F 1*s* core electrons (Fig. 4b) for the anatase single crystals clearly matches the model description in Fig. 1a–d; the measured binding energy is only 684.5 eV, which is a typical value for fluorated TiO_2 systems such as $TiOF_2$ or the surface Ti–F species[29]. Furthermore, the oxidation state of the Ti element in the same materials (Ti $2p_{3/2}$, binding energy 458.8 eV; Ti $2p_{1/2}$, binding energy 464.3 eV) is identical to that of bulk TiO_2, as reported previously[30]. From the X-ray photoelectron spectroscopy results, we can conclude that the atomic incorporation of F atoms, or their substitution for O atoms, in the anatase TiO_2 crystal lattice (doping) can be ruled out. These results strongly support the initial theoretical predictions and our explanation in terms of surface atoms; that is, the high F–Ti bonding energy significantly lowers the energy of the (001) surfaces, making them more stable than (101) surfaces in our reaction media. Importantly, the fluorated surfaces of anatase single crystals can easily be made clean, fluorine-free surfaces by heating at 600 °C for 90 min, without changing their crystal structure and morphology (Supplementary Fig. 8).

The well-defined, high-purity anatase single crystals synthesized in this work would be very useful as model single crystals for fundamental studies in surface science. Furthermore, high-purity anatase single crystals with a high percentage of reactive {001} facets have promising applications in solar cells, photonic and optoelectronic devices, sensors and photocatalysis. Our results illustrate the power of combining first-principle calculations and experimental techniques to achieve engineering of surface and crystallographic characteristics of crystalline materials.

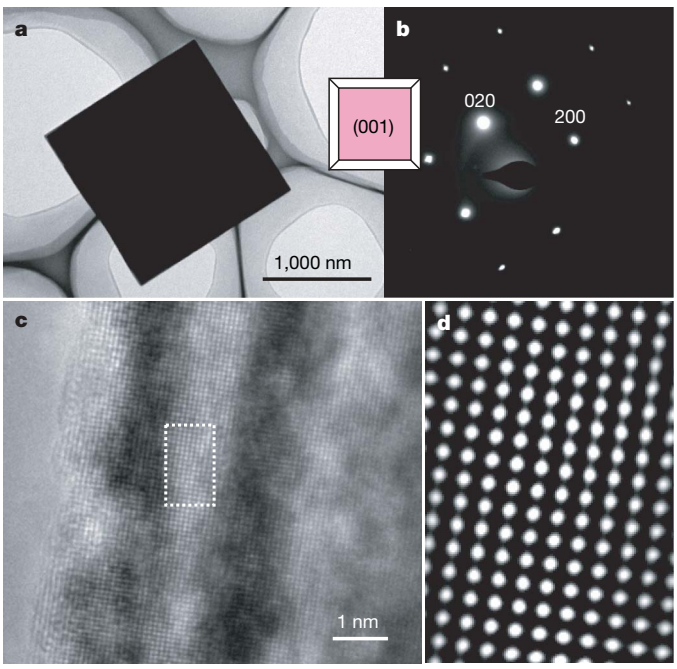

Figure 3 | Crystalline phase determination. **a**, Bright-field TEM image of a representative anatase single crystal recorded along the [001] axis. **b**, Presence of the anatase single-crystal phase can be confirmed by the square-symmetric selected-area electron diffraction pattern. Inset is a [001]-projected geometrical model of the anatase single crystals. **c**, High-resolution TEM image recorded from another anatase single crystal with [001] orientation. **d**, Fast-Fourier-transform-filtered TEM image recorded from the dotted rectangular area in **c**.

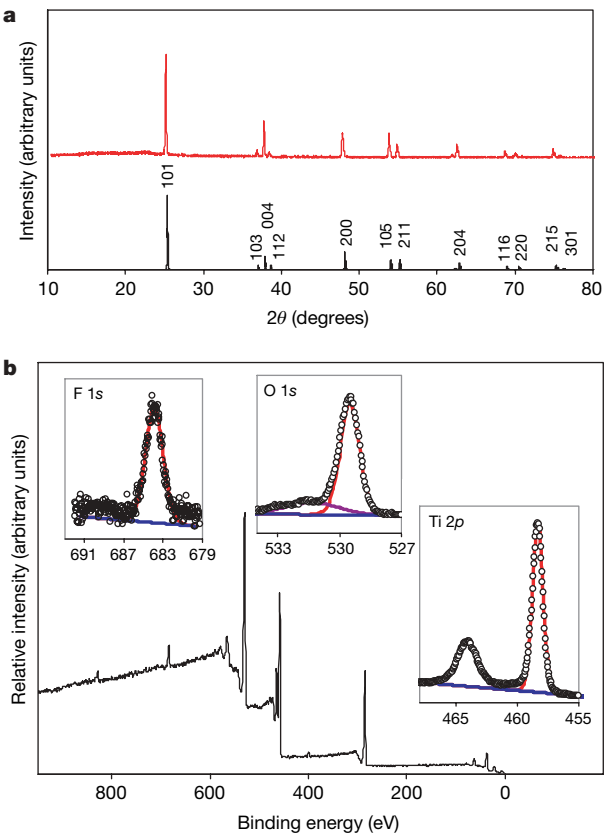

Figure 4 | Confirmation of the spatial distribution of F atoms in anatase single crystals. **a**, A representative X-ray diffraction pattern of the anatase single crystals we synthesized in this work (red), which is in good agreement with the calculated diffraction pattern of bulk anatase (black). θ, diffraction angle. **b**, X-ray photoelectron spectra of anatase single crystals, showing the four characteristic peaks of Ti, O, F and C. The insets have the same axes as the main panel. The open circles are the raw data of the X-ray photoelectron spectra, and the blue and red/purple lines represent the base line and fitted lines, respectively.

METHODS SUMMARY

Theoretical. Surface free energies were calculated using density functional theory within the generalized-gradient approximation. In each case, stoichiometric slab models (1×1) were employed, with all atoms being relaxed without any constraint.

Experimental. Titanium tetrafluoride aqueous solution (varying in concentration between 2.67 and 5.33 mM) and hydrofluoric acid (10 wt%) were used as the precursor and the crystallographic controlling agent, respectively, to prepare anatase TiO_2 single crystals. The reaction was carried out in a Teflon-lined autoclave at 180 °C for 2 to 20 h.

Full Methods and any associated references are available in the online version of the paper at www.nature.com/nature.

Received 26 November 2007; accepted 1 April 2008.

1. Tian, N., Zhou, Z. Y., Sun, S. G., Ding, Y. & Wang, Z. L. Synthesis of tetrahexahedral platinum nanocrystals with high-index facets and high electro-oxidation activity. *Science* **316,** 732–735 (2007).
2. Bikondoa, O. *et al.* Direct visualization of defect-mediated dissociation of water on TiO_2 (110). *Nature Mater.* **5,** 189–192 (2006).
3. Dulub, O. *et al.* Electron-induced oxygen desorption from the TiO_2 (011)-2×1 surface leads to self-organized vacancies. *Science* **317,** 1052–1056 (2007).
4. Gong, X. Q., Selloni, A., Batzill, M. & Diebold, U. Steps on anatase TiO_2 (101). *Nature Mater.* **5,** 665–670 (2006).
5. Diebold, U. The surface science of titanium dioxide. *Surf. Sci. Rep.* **48,** 53–229 (2003).
6. Thomas, A. G. *et al.* Resonant photoemission of anatase TiO_2 (101) and (001) single crystals. *Phys. Rev. B* **67,** 035110 (2003).
7. Kavan, L., Grätzel, M., Gilbert, S. E., Klemenz, C. & Scheel, H. J. Electrochemical and photoelectrochemical investigation of single-crystal anatase. *J. Am. Chem. Soc.* **118,** 6716–6723 (1996).
8. Gong, X. Q. & Selloni, A. Reactivity of anatase TiO_2 nanoparticles: the role of the minority (001) surface. *J. Phys. Chem. B* **109,** 19560–19562 (2005).
9. Herman, G. S., Sievers, M. R. & Gao, Y. Structure determination of the two-domain (1×4) anatase TiO_2(001) surface. *Phys. Rev. Lett.* **84,** 3354–3357 (2000).
10. Lazzeri, M., Vittadini, A. & Selloni, A. Structure and energetics of stoichiometric TiO_2 anatase surfaces. *Phys. Rev. B* **63,** 155409 (2001).
11. Vittadini, A., Selloni, A., Rotzinger, F. P. & Grätzel, M. Structure and energetics of water adsorbed at TiO_2 anatase (101) and (001) surfaces. *Phys. Rev. Lett.* **81,** 2954–2957 (1998).
12. Vittadini, A., Casarin, M. & Selloni, A. Chemistry *of* and *on* TiO_2-anatase surfaces by DFT calculations: a partial review. *Theor. Chem. Acc.* **117,** 663–671 (2007).
13. Lazzeri, M. & Selloni, A. Stress-driven reconstruction of an oxide surface: the anatase TiO_2(001)-(1×4) surface. *Phys. Rev. Lett.* **87,** 266105 (2001).
14. Fujishima, A. & Honda, K. Electrochemical photolysis of water at a semiconductor electrode. *Nature* **238,** 37–38 (1972).
15. O'Regan, B. & Grätzel, M. A low-cost, high-efficiency solar cell based on dye-sensitized colloidal TiO_2 films. *Nature* **353,** 737–740 (1991).
16. Grätzel, M. Photoelectrochemical cells. *Nature* **414,** 338–344 (2001).
17. Barbé, C. J. *et al.* Nanocrystalline titanium oxide electrodes for photovoltaic applications. *J. Am. Ceram. Soc.* **80,** 3157–3171 (1997).
18. Penn, R. L. & Banfield, J. F. Morphology development and crystal growth in nanocrystalline aggregates under hydrothermal conditions: Insights from titania. *Geochim. Cosmochim. Acta* **63,** 1549–1557 (1999).
19. Zaban, A., Aruna, S. T., Tirosh, S., Gregg, B. A. & Mastai, Y. The effect of the preparation condition of TiO_2 colloids on their surface structures. *J. Phys. Chem. B* **104,** 4130–4133 (2000).
20. Jun, Y. W. *et al.* Surfactant-assisted elimination of a high energy facet as a means of controlling the shapes of TiO_2 nanocrystals. *J. Am. Chem. Soc.* **125,** 15981–15985 (2003).
21. Barnard, A. S. & Curtiss, L. A. Prediction of TiO_2 nanoparticle phase and shape transitions controlled by surface chemistry. *Nano Lett.* **5,** 1261–1266 (2005).
22. Chen, X. & Mao, S. S. Titanium dioxide nanomaterials: synthesis, properties, modifications, and applications. *Chem. Rev.* **107,** 2891–2959 (2007).
23. Izumi, F. The polymorphic crystallization of titanium (IV) oxide under hydrothermal conditions. II. The roles of inorganic anions in the nucleation of rutile and anatase from acid solutions. *Bull. Chem. Soc. Jpn* **51,** 1771–1776 (1978).
24. Berger, H., Tang, H. & Lévy, F. Growth and Raman spectroscopic characterization of TiO_2 anatase single crystals. *J. Cryst. Growth* **130,** 108–112 (1993).
25. Zmbov, K. F. & Margrave, J. L. Mass spectrometric studies at high temperatures. XVI. Sublimation pressures for TiF_3 (g) and the stabilities of TiF_2 (g) and TiF (g). *J. Phys. Chem.* **71,** 2893–2895 (1967).
26. Huber, K. P. & Herzberg, G. in *Molecular Spectra and Molecular Structure. IV. Constants of Diatomic Molecules* 642 (Van Nostrand Reinhold, New York, 1979).
27. Barnard, A. S. & Zapol, P. A model for the phase stability of arbitrary nanoparticles as a function of size and shape. *J. Chem. Phys.* **121,** 4276–4283 (2004).
28. Yang, H. G. & Zeng, H. C. Preparation of hollow anatase TiO_2 nanospheres via Ostwald ripening. *J. Phys. Chem. B* **108,** 3492–3495 (2004).
29. Yu, J. C., Yu, J., Ho, W., Jiang, Z. & Zhang, L. Effects of F^- doping on the photocatalytic activity and microstructures of nanocrystalline TiO_2 powders. *Chem. Mater.* **14,** 3808–3816 (2002).
30. Lou, X. W. & Zeng, H. C. Complex α-MoO_3 nanostructures with external bonding capacity for self-assembly. *J. Am. Chem. Soc.* **125,** 2697–2704 (2003).

Supplementary Information is linked to the online version of the paper at www.nature.com/nature.

Acknowledgements This work was supported by the Australian Research Council. H.G.Y. wishes to express his gratitude to the National University of Singapore, where the preliminary experimental work was carried out. The authors acknowledge Qiu Hong Hu for her help with statistical analysis.

Author Information Reprints and permissions information is available at www.nature.com/reprints. Correspondence and requests for materials should be addressed to G.Q.L. (maxlu@uq.edu.au) or S.Z.Q (s.qiao@uq.edu.au).

METHODS

Theoretical calculations. In each calculation, stoichiometric slab models (1×1) were used, consisting of nine atomic layers and a total of nine atoms for clean (001) surfaces and eight atomic layers and a total of 12 atoms for clean (101) surfaces. Each of these (001) and (101) surfaces contains one fivefold Ti atom terminated by an X atom (where X represents H, B, C, N, O, F, Si, P, S, Cl, Br or I). All atoms were relaxed without any constraint. All calculations were carried out using density functional theory within the generalized-gradient approximation[31], with the exchange-correlation functional of ref. 32 (see also ref. 33). This was implemented in the Vienna *ab initio* simulation package[34,35], which spans reciprocal space with a plane-wave basis, in this case up to a kinetic energy cutoff of 450 eV. We used an $11 \times 11 \times 11$ Monkhorst–Pack *k*-point mesh for bulk anatase, an $11 \times 11 \times 1$ mesh for slabs, and a $3 \times 3 \times 3$ mesh for dimers of X for final calculations of energies. During the relaxations, all structures were relaxed to an energy convergence of 10^{-4} eV (equating to a force convergence of 10^{-2} eV Å^{-1}). In the case of slabs, the vacuum space is larger than 15 Å, and for the dimers of X a cubic unit cell with $a = b = c = 16$ Å was used. For isolated atoms (to correct the cohesive energy), a unit cell with $a = 15$ Å, $b = 16$ Å and $c = 17$ Å was used.

Synthesis of anatase TiO_2 single crystals. Hydrochloric acid (1.5 M) was used to adjust the pH of deionized water (1.0 l) to around 2.1. Titanium tetrafluoride (TiF_4, Aldrich Chemical) was then dissolved in this solution to a concentration of 0.04 M, which changed the pH to 1.8 (refs 36, 37). Finally, deionized water was used to adjust the concentration of TiF_4 aqueous solution to a concentration of 2.67 to 5.33 mM. In a typical synthesis, 30 ml of TiF_4 aqueous solution and 0.4 ml of hydrofluoric acid (10 wt%) were added to a Teflon-lined autoclave and a transparent mixture formed; the mixture was kept at 180 °C for 2 to 20 h in an oven. After completion of the reaction, the clear solution at the upper section was carefully removed by plastic dropper and a precipitate (TiO_2 product) formed at the bottom of the Teflon reactor. The solid products obtained were washed three times with deionized water (15 ml each time) and then dried at 100 °C or redispersed in deionized water for further characterization.

Fluorine removal from the surface of anatase TiO_2 single crystals. Typically, the powder samples of as-prepared anatase TiO_2 single crystals were heat treated in static air in a Muffle furnace at temperatures of 200 to 600 °C for 90 min with a ramping rate of 5 °C min^{-1}. The samples were then cooled to room temperature in the Muffle furnace, for further characterization.

Materials characterization. Crystallographic information of anatase TiO_2 single crystals was obtained with X-ray diffraction (Shimadzu XRD-6000, Cu Kα radiation). Chemical compositions of anatase TiO_2 single crystals were analysed using X-ray photoelectron spectroscopy (Kratos Axis ULTRA incorporating a 165 mm hemispherical electron-energy analyser). All binding energies were referenced to the C 1*s* peak (285.0 eV) arising from adventitious carbon. Prior peak deconvolution, X-ray satellites and inelastic background (Shirley-type) were subtracted for all spectra. Morphology and crystal structure of anatase TiO_2 single crystals were examined using SEM (JEOL JSM6400F & JSM890) and TEM (Philips Tecnai T12 and T30F FEG Cryo AEM). Samples of anatase TiO_2 single crystals were dispersed in deionized water and dropped on a conductive SEM sample holder, or a carbon-coated copper grid with irregular holes for electron microscopy (SEM/TEM) analysis. X-ray photoelectron spectroscopy and X-ray diffraction samples were prepared by drying the sedimented particles overnight at 100 °C.

31. Kohn, W. & Sham, L. J. Self-consistent equations including exchange and correlation effects. *Phys. Rev. B* **140,** A1133–A1138 (1965).
32. Perdew, J. P., Burke, K. & Ernzerhof, M. Generalized gradient approximation made simple. *Phys. Rev. Lett.* **77,** 3865–3868 (1996).
33. Kresse, G. & Joubert, D. From ultrasoft pseudopotentials to the projector augmented-wave method. *Phys. Rev. B* **59,** 1758–1775 (1999).
34. Kresse, G. & Furthmüller, J. Efficient iterative schemes for ab initio total-energy calculations using a plane-wave basis set. *Phys. Rev. B* **54,** 11169–11186 (1996).
35. Kresse, G. & Furthmüller, J. Efficiency of ab-initio total energy calculations for metals and semiconductors using a plane-wave basis set. *Comput. Mater. Sci.* **6,** 15–50 (1996).
36. Yang, H. G. & Zeng, H. C. Creation of intestine-like interior space for metal-oxide nanostructures with a quasi-reverse emulsion. *Angew. Chem. Int. Ed.* **43,** 5206–5209 (2004).
37. Yang, H. G. & Zeng, H. C. Synthetic architectures of $TiO_2/H_2Ti_5O_{11}{\cdot}H_2O$, $ZnO/H_2Ti_5O_{11}{\cdot}H_2O$, $ZnO/TiO_2/H_2Ti_5O_{11}{\cdot}H_2O$ and ZnO/TiO_2 nanocomposites. *J. Am. Chem. Soc.* **127,** 270–278 (2005).